Advances in Water Resources 96 (2016) 290–305

Contents lists available at ScienceDirect

Advances in Water Resources

journal homepage: www.elsevier.com/locate/advwatres

Raindrop size distribution: Fitting performance of common theoretical models

E. Adirosi[a,*], E. Volpi[b], F. Lombardo[b], L. Baldini[a]

[a] Institute of Atmospheric Sciences and Climate (ISAC), National Research Council of Italy (CNR), Rome, Italy
[b] Dipartimento di Ingegneria, Università degli Studi Roma Tre, Rome, Italy

ARTICLE INFO

Article history:
Received 29 February 2016
Revised 17 June 2016
Accepted 18 July 2016
Available online 4 August 2016

Keywords:
Drop size distribution
Maximum likelihood method
Kolmogorov–Smirnov test
Model selection

ABSTRACT

Modelling raindrop size distribution (DSD) is a fundamental issue to connect remote sensing observations with reliable precipitation products for hydrological applications. To date, various standard probability distributions have been proposed to build DSD models. Relevant questions to ask indeed are how often and how good such models fit empirical data, given that the advances in both data availability and technology used to estimate DSDs have allowed many of the deficiencies of early analyses to be mitigated. Therefore, we present a comprehensive follow-up of a previous study on the comparison of statistical fitting of three common DSD models against 2D-Video Distrometer (2DVD) data, which are unique in that the size of individual drops is determined accurately. By maximum likelihood method, we fit models based on lognormal, gamma and Weibull distributions to more than 42.000 1-minute drop-by-drop data taken from the field campaigns of the NASA Ground Validation program of the Global Precipitation Measurement (GPM) mission. In order to check the adequacy between the models and the measured data, we investigate the goodness of fit of each distribution using the Kolmogorov–Smirnov test. Then, we apply a specific model selection technique to evaluate the relative quality of each model. Results show that the gamma distribution has the lowest KS rejection rate, while the Weibull distribution is the most frequently rejected. Ranking for each minute the statistical models that pass the KS test, it can be argued that the probability distributions whose tails are exponentially bounded, i.e. light-tailed distributions, seem to be adequate to model the natural variability of DSDs. However, in line with our previous study, we also found that frequency distributions of empirical DSDs could be heavy-tailed in a number of cases, which may result in severe uncertainty in estimating statistical moments and bulk variables.

1. Introduction

Accurate measurement of precipitation is of fundamental importance in hydrology as well as in several Earth science disciplines. Precipitation can produce floods and trigger landslides, which cause annually loss of lives and damages (Trenberth 2011, Trezzini et al., 2013). Indeed, the precipitation amount is the main input to rainfall-runoff models and plays a significant role in the design of most of the hydraulic structures. Therefore, accurate knowledge, understanding and measurement of precipitation and its variability in both space and time is strongly needed by several critical applications.

Precipitation can be directly measured by ground-based pointwise devices, such as rain gauges and disdrometers, or estimated by remote sensing techniques using satellite or airborne passive or active microwave sensors or ground-based weather radar. Remote sensing techniques obtain indirect measurements of rainfall, which are of great importance for process understanding and characterization thanks to the wide spatial coverage, and are the primary source of observations in ungauged regions. However, indirect measurements are generally affected by a variety of potential sources of uncertainty that can be related to both instrumental errors and conversion of measurements into rainfall rate at the ground level (Stephens and Kummerow, 2007; Brandes et al., 1999; Villarini and Krajevski, 2010; Sebastianelli et al., 2013 among others).

Quantitative Precipitation Estimates (QPE) from remote sensing measurements can be significantly improved through an accurate characterization and modelling of the Drop Size Distribution (DSD), which is involved in the development of rainfall retrieval algorithms (Villarini and Krajevski, 2010; Rose and Chandrasekar, 2006; Kozu et al., 2009). A reliable DSD estimate plays also an important role in numerical weather prediction (NWP) models;

* Corresponding author at: Consiglio Nazionale delle Ricerche, Istituto di Scienze dell'Atmosfera e del Clima, Area della Ricerca Roma 2 "Tor Vergata", Via Fosso del Cavaliere, 100, I-00133 Roma, Italy.
E-mail address: elisa.adirosi@artov.isac.cnr.it (E. Adirosi).

http://dx.doi.org/10.1016/j.advwatres.2016.07.010
0309-1708/

indeed, varying the DSD shape can highly change the precipitation amount and the intensity in simulated storms (van den Heever and Cotton 2004).

On the basis of the above considerations, it is easily understood that characterizing and modelling DSDs are indeed receiving renewed research interest (D'Adderio et al., 2015; Cugerone and De Michele, 2015; Ekerete et al., 2015; Adirosi et al., 2016; Brown et al., 2016; Jameson and Larsen, 2016; Marzuki et al., 2016; Suh et al., 2016).

The DSD is defined to be the number of drops per unit volume of air and per unit of drop diameter interval. It results from several physical and microphysical complex phenomena involved in the generation and evolution of rain; therefore, the DSD shape can present a high variability both in space and in time, thus reflecting the variability of rainfall. Starting from the seminal work of Marshall and Palmer (1948), who used dyed filter papers, many field campaigns have been conducted worldwide with different measuring devices, mainly from a category of instruments called disdrometers (Kathiravelu et al., 2016). Based on the collected data, different DSD parameterizations have been reported in the literature (see e.g. Adirosi et al., 2015 and references therein), considering also different climate regions or rain types (see e.g. Awang and Din 2004).

Statistical frequency analysis procedures postulate some kind of model for the process that generates empirical data. Concerning precipitation microstructure, like most environmental data, the actual data-generating mechanism is so complicated that we cannot expect the model to be an exact representation of the physical process. Therefore, we believe it is wise to consider as candidate frequency distributions a range of probability distributions allowing for both parsimonious parameterization and simple analytical calculation of statistical moments and bulk variables, which are important motivations for practical applications. A problem with this approach is that available sample sizes are usually not so large that the frequency distribution can be identified unequivocally in such a way as to represent all the different conditions generally met in nature. For example, failure to detect that the DSD is heavy-tailed, will result in severe uncertainty in the retrieval of bulk variables for hydrological applications (Adirosi et al., 2015). Therefore, major improvements in DSD estimation are anticipated in the near future, as disdrometer data will become more reliable and will accumulate in time providing datasets with lengths adequate to enable reliable investigation of the probability distribution of drop sizes. This paper reports some progress in this respect.

In recent years, an increasing complexity in DSD models has been proposed with the aim of using distributions with enough free parameters that they can mimic a wide range of plausible frequency distributions (Ekerete et al., 2015; Cugerone and De Michele, 2015). However, an increase in complexity will introduce more model data and parameter requirements, where both data and parameters are uncertain (see e.g. Perrin et al., 2001; Schoups et al., 2008). Hence, the use of highly parameterized models can enhance the estimation uncertainty that usually characterizes DSD estimates from disdrometer data. As suggested by Marzuki et al. (2012), the rainfall properties estimated from disdrometer data are indeed affected by a large variability that can be related not only to climatological and physical factors but also to instrumental factors. Specifically, they show that the disdrometer limitations (resolution and sensitivity), its under-sampling effect and the discretization procedure that provides binned data at a given discretization interval, generate errors when estimating the DSD from observed data.

As follow-up of a previous study (Adirosi et al., 2015), this paper aims at evaluating the performance of the three different distributions adopted in the DSD modelling literature, i.e. gamma, lognormal and Weibull distributions, in representing raindrop size distributions in nature. This is achieved by applying a statistical analysis to large datasets disdrometer-measured drop size spectra. In fact, although the gamma is the most widely adopted distribution to model the natural DSD, also the lognormal and the Weibull distributions have been considered (see Adirosi et al., 2015 and references therein) and a study trying to evaluate in a rigorous manner at what extent such distributions are able to represent the natural variability of DSD is still lacking. We consider herein only distributions with two parameters in order to limit the estimation uncertainty and to take into account the fact that more parameters are hardly retrievable from the limited independent measurements usually available from remote sensing sensors (see e.g. Williams et al., 2014).

This study is based on an up-to-date statistical approach, which supports the absolute statistical performance of the theoretical distributions mentioned above. Indeed, our analysis of the DSD is carried out by fitting standard probability distributions to raindrop data and testing their goodness of fit. In the literature, goodness of fit is usually assessed via the accuracy of the rainfall or other predictions derived from the DSD or by the relative ranking of models, while only recent studies have used absolute tests (Ekerete et al., 2015; Cugerone and De Michele, 2015). In this paper, we also test the absolute fit, whether the proposed model fits the data, using the common Kolmogorov–Smirnov test. In such an analysis, we explicitly take into account the role of the relationship between the drop terminal fall velocity and diameter, in order to evaluate how the assumption of a certain functional form for the drop velocity may affect the shape of the DSD.

We wish to emphasize that, differently from other works in the literature, our analysis is based on high quality datasets recorded by 2D Video Disdrometers (2DVD) (Kruger and Krajewski, 2002; Schönhuber et al., 2008). Such instruments provide more accurate and richer information with respect to other types of disdrometers, thus allowing to potentially reduce the estimation uncertainty that is usually related to the instrumental limitations (Marzuki et al., 2012). In fact, the 2DVD directly measures the diameter and terminal fall velocity of each single hydrometeor that falls through its sampling area instead of providing data binned in predefined particle size classes. Moreover, although other types of disdrometer are more sensitive to small drops, the 2DVD allows for a more accurate estimate in a wider range of drop sizes, including the larger drops (Tokay et al., 2013; Gatlin et al., 2015).

Thousands of 1-minute disdrometer data collected at different locations in the world have been considered to investigate extensively the drop size distribution of rainfall. It is worth noting that the 2DVD spectra have been collected during four different pre-launch field campaigns of the Ground Validation program of the NASA-Jaxa Global Precipitation Measurement (GPM) mission (Hou et al., 2014) in four different regions, namely Italy, Oklahoma, Iowa and Appalachian Mountains (see Section 4). We highlight that we include an additional dataset with respect to Adirosi et al. (2015). Therefore, the outcomes presented in this study are not site-specific.

The remainder of this paper is organized as follows. Section 2 provides some insight into definition and mathematical formulation of the DSD from the statistical point of view. Furthermore, in this Section we theoretically analyze the role of the terminal fall velocity of the drops in the computation of the DSD. Section 3 explains the methodology followed in this study to fit the measured drop spectra – with and without taking into account the relationship between the drop terminal fall velocity and size and considering both complete and truncated distributions – and to test and select the fitted models. A brief description of the measured datasets is provided in Section 4, while Section 5 illustrates the main results and their implications from a practical perspective. Finally, a conclusion Section 6 closes the paper.

2. Mathematical framework

2.1. DSD definitions and relationships

From a statistical point of view, and following the definition given in the Introduction, the drop size distribution can be expressed as the product of the concentration of the raindrops in a volume of air (n_c in m^{-3}) by the probability distribution of drop sizes in the unit volume of air, $f_V(D)$ (mm^{-1})

$$N(D) = n_c \; f_V(D) \tag{1}$$

We assume that $f_V(D)$ can be represented mathematically by the lognormal, gamma and Weibull distributions. It is worth noting that, for disdrometer measurements, the volume of air V (m^3) which the DSD refers to is proportional to the disdrometer sampling time interval Δt (s), the measuring area A (m^2), and the terminal fall speed of the drops $v(D)$ (m s^{-1}), which is related to the drop diameter, i.e. $V = \Delta t \; A \; v(D)$.

The variability of raindrop sizes can be also expressed in terms of the product of the probability density function of drop diameters at the ground, $f(D)$ (mm^{-1}) by the number M of drops collected at ground. Hence, the probability distribution of drop diameter in the unit volume of air, $f_V(D)$ is linked to the distribution of drop sizes at ground, $f(D)$, such as (Ignaccolo and De Michele, 2014)

$$n_c f_V(D) = \frac{M f(D)}{A \Delta t \, v(D)} \tag{2}$$

Since $f_V(D)$ – as well as $f(D)$ – is a proper probability density function (pdf), such that $\int_0^\infty f_V(D)dD = 1$, using Eq. (2) and exploiting the latter $f_V(D)$ property we can derive the expression for the concentration of the raindrops in a volume of air n_c as a function of the total number M of drops collected at ground

$$n_c = \frac{M}{A \; \Delta t} \int_0^\infty \frac{f(D)}{v(D)} dD. \tag{3}$$

Then, by substituting Eq. (3) in Eq. (2), we obtain

$$f_V(D) = \frac{f(D) v(D)^{-1}}{\int_0^\infty f(D) v(D)^{-1} dD}. \tag{4}$$

It also follows that

$$f(D) = \frac{f_V(D) v(D)}{\int_0^\infty f_V(D) v(D) dD}. \tag{5}$$

Eq. (4) shows that, while $f(D)$ only depends on the diameter values, the shapes of $f_V(D)$ and $N(D)$ as per Eq. (1) strictly depend on the relationship between the drop fall velocity and diameter $v(D)$. The theoretical role of the terminal fall velocity-diameter relationship is analyzed in detail in the following section.

2.2. Role of the terminal fall velocity v(D)

Even if most disdrometers can measure the arrival velocity of the falling drops, a theoretical relationship between the terminal fall velocity and the drop diameter is usually adopted for DSD computation (see e.g. Kruger and Krajewski, 2002; Caracciolo et al., 2006; Marzuki et al., 2013; Adirosi et al., 2014; Angulo-Martinez and Barros, 2015 and Adirosi et al. 2015 among others). Many size-fall velocity relationships are reported in the literature (see e.g. Atlas et al., 1973; Beard, 1976; Atlas and Ulbrich, 1977; Brandes et al. 2002 among others). Some laboratory and empirical experiments have been carried out to measure the drop terminal fall velocity (e.g. Laws, 1941; Gunn and Kinzer, 1949; Beard and Pruppacher, 1969 and more recently Thurai and Bringi, 2005). Atlas and Ulbrich (1977) proposed a power-law relationship, such as

$$v(D) \; = \; 3.78 \; D^{0.67} \tag{6}$$

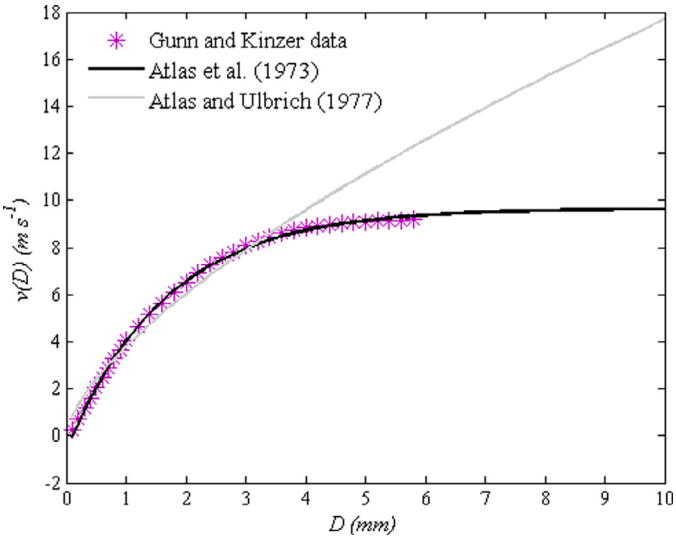

Fig. 1. Raindrop terminal fall speed as a function of diameter. Observations of Gunn and Kinzer (1949) are shown as black stars markers. The Atlas et al. (1973) relation is the dark gray solid curve and the Atlas and Ulbrich (1977) power-law relation is the light gray solid line.

(with D in mm and v in mm s^{-1}), that is valid for D ranging from 0.5 mm to 5 mm, while Atlas et al. (1973) obtained the following relation:

$$v(D) = 9.65 - 10.3 \; e^{-0.6D} \tag{7}$$

The two size-velocity models in (6) and (7) are based on the experimental work of Gunn and Kinzer (1949), but are also a good approximation to the data collected in the experiment by Thurai and Bringi (2005) considering drops falling from a bridge 80 m above the disdrometer. The Atlas et al. (1973) and Atlas and Ulbrich (1977) relations together with the Gunn and Kinzer (1949) data are shown in Fig. 1. The deviation of the Atlas and Ulbrich (1977) relation from the experimental data is evident for D greater than about 4 mm, therefore Atlas et al. (1973) fit seems to better approximate the data, although for very small drops ($D \lesssim 0.11$ mm) it has the problem to output negative values. Please note that the latter relations should need an altitude correction in the case of high altitude locations (Beard, 1985).

The choice of the theoretical relationship, e.g. between those of Atlas and Ulbrich (1977) and Atlas et al. (1973) given in Eqs. (6) and (7) respectively, has some important implications on DSD estimation. Indeed, the functional form of $v(D)$ can modify the shape of $f_V(D)$ with respect to that of $f(D)$. Ignaccolo and De Michele (2014) demonstrated that if $f_V(D)$ is a gamma distribution, i.e. $f_V(D) = p_\Gamma(D; \lambda, \mu)$ where

$$p_\Gamma(D; \lambda, \mu) = \frac{D^\mu e^{-D\lambda} \lambda^{\mu+1}}{\Gamma[\mu + 1]} \tag{8}$$

as it is commonly assumed in practical applications, then also the $f(D)$ follows a gamma distribution with the same scale parameter λ and a shape parameter related to that of $f_V(D)$ by a simple linear relation (Ignaccolo and De Michele 2014, Eq. (12))

$$f(D) = p_\Gamma(D; \lambda, \mu + 0.67) \tag{9}$$

However, the latter statement holds true only if we adopt a power-law relationship between the drop fall velocity and the drop diameter, such as Eq. (6). By contrast, if we hold Eq. (7) because it describes more appropriately the velocity of larger drops (Thurai and Bringi, 2005), and then substitute Eqs. (7) and (8) in Eq. (5) we obtain

$$f(D) = \frac{p_\Gamma(D; \lambda + 0.6, \mu) + \gamma(\lambda, \mu) \; p_\Gamma(D; \lambda, \mu)}{1 + \gamma(\lambda, \mu)} \tag{10}$$

where $\gamma(\lambda,\mu) = -10.33/9.65(\lambda/(\lambda+0.6))^{\mu+1}$. By Eq. (10), $f(D)$ is nothing else than the linear combination of two gamma distributions. The difference between the pdfs expressed by Eqs. (9) and (10) clearly depends on the parameter values, and it might be not negligible in the ranges of parameter values commonly used for DSD modelling.

3. Methods

3.1. DSD estimation from disdrometer data

The "instantaneous" drop size distribution is usually estimated from data collected by disdrometers with a sampling interval $\Delta t =$ 1 min. Depending on the device measurement principle, there are disdrometers (i) that provide the number of drops (n_i) within a predefined size (ΔD) and fall velocity bins (Δv), with $i = 1, 2, \ldots, M_D$, where M_D is the total number of size and velocity classes. Other devices (ii), such as the 2DVD, detect the diameter and fall velocity of each single drop passing through the virtual measuring area, without grouping the data into classes.

Once the measurements are collected, the empirical drop size distribution can be calculated in the case (i) as

$$N(\bar{D}_i) = \frac{n_i}{\Delta D\, \Delta t\, A\, v(D)} \tag{11}$$

where $\bar{D}_i$ is a nominal drop diameter that corresponds to the mean of the ith bin width. The overall sum of the number of drops n_i, for $i = 1, \ldots, M_D$, equals the number of drops collected at the ground M. Otherwise, case (ii), the empirical DSD can be estimated starting from the empirical frequency of the diameter sample, $\mathbf{D} = \{D_j\}$ with $j = 1, \ldots, M$ (M gives the sample size).

In our work, we estimate the pdfs $f(D)$ and $f_V(D)$ from drop-by-drop data, without binning. The statistical methodologies for the estimation of $f(D)$ and $f_V(D)$ are further illustrated in the following Section.

3.2. Statistical inference of f(D) and f_V(D)

In this study, three different two-parameter continuous distributions related to positive, real-valued quantities (i.e. raindrop diameters), are fitted to the disdrometer-measured drop size spectra by the Maximum Likelihood method (ML) (Haddad et al., 1996; Marzuki et al., 2012). In the literature, the method of moments (MM) is broadly used for DSD estimation (e.g. Waldvogel, 1974; Ulbrich, 1983; Tokay and Short, 1996; Ulbrich and Atlas, 1998; Szyrmer et al., 2005 among others). Nevertheless, recent works have criticized MMs for producing biased parameters, whereas the maximum likelihood method proves to perform better (see e.g. Smith and Kliche, 2005; Smith et al., 2009; Kliche et al., 2008).

As shown above, the pdfs $f(D)$ and $f_V(D)$ are transformations of one another. Therefore, it is possible to estimate the former from data and then derive the latter or vice versa. When fitting the probability distribution of drop diameters at the ground $f(D)$ to data, the model parameters can be estimated by maximizing the classical likelihood function

$$\mathcal{L}(\beta,\gamma) = \prod_{i=1}^{M} [p(D_i;\beta,\gamma)] \tag{12}$$

where $p(D_i;\ \beta,\ \gamma)$ denotes the probability model with scale parameter β and shape parameter γ. Otherwise, when we wish to estimate the probability distribution of drop sizes in the unit volume of air, $f_V(D)$, the likelihood function becomes (Haddad et al., 1996)

$$\mathcal{L}(\beta,\gamma) = \prod_{i=1}^{M} [p(D_i;\beta,\gamma)]^{N_i} \tag{13}$$

where β and γ are respectively the scale and shape parameters of $f_V(D)$, and N_i is obtained from the drop-by-drop data basis. The latter quantity is simply given by the inverse of the volume of air, V, as defined above and considering the size-velocity relationship in Eq. (7).

In the hydro-meteorological literature, the use of the definition of drop size distribution given in (1) prevails, and, except for few studies, all of the proposed fitting methods aim to model the $f_V(D)$. Therefore, in order to provide results and considerations that can be useful and easily applicable in the practice, we focus our analysis on the direct fitting of $f_V(D)$. Notwithstanding this, some results of the fitting of $f(D)$ are also provided herein in order to highlight the role of $v(D)$ in DSD estimation and analyze results from a different perspective.

The theoretical distributions considered in this study are the models mostly adopted in the literature: gamma (GA), lognormal (LN) and Weibull (WE) distributions with positive shape and scale parameters, i.e. $\beta,\ \gamma > 0$. Revising Eq. (1) in terms of such distributions, we have

$$N_{GA}(D) = n_c\ p_{GA}(D) = n_c\ \frac{1}{\beta\ \Gamma(\gamma)} \left(\frac{D}{\beta}\right)^{\gamma-1} \exp(-D/\beta) \tag{14}$$

$$N_{LN}(D) = n_c\, p_{LN}(D) = n_c \frac{1}{D\gamma\sqrt{\pi}} \exp\left[-\ln^2(D/\beta)^{\frac{1}{\gamma}}\right] \tag{15}$$

$$N_{WE}(D) = n_c\, p_{WE}(D) = n_c \frac{\gamma}{\beta} \left(\frac{D}{\beta}\right)^{\gamma-1} \exp(-D/\beta)^{\gamma} \tag{16}$$

In the fitting procedure, n_c is determined by imposing that the total predicted drop concentration matches the total expected drop concentration, and the two other parameters (i.e. the shape and scale parameters) are estimated by maximum likelihood method (Haddad et al., 1996). Note that the gamma distribution used by the meteorological community to describe the natural DSD has typically the form (Ulbrich, 1983)

$$N_{GA}(D) = n_c\ \frac{\Lambda^{\mu+1}}{\Gamma(\mu+1)}\ D^{\mu} \exp(-\Lambda D) = N_o D^{\mu} \exp(-\Lambda D) \tag{17}$$

which is equivalent to Eq. (14) letting $\mu = \gamma - 1$ and $\Lambda = 1/\beta$.

It is important to recall that current disdrometers have some limitations in detecting smaller drops. Specifically the 2DVD is not able to detect accurately the drops with diameter smaller than about 0.2 mm (Tokay et al., 2013). Consequently, the number of small raindrops is probably underestimated by these devices. In order to take into account the lack of small drops due to instrumental limitations, the Truncated Maximum Likelihood method (TML) can be applied (see e.g. Mallet and Barthes, 2009; Johnson et al., 2014). Following this approach, the model parameters of the probability distribution of drop diameters at the ground $f(D)$ can be estimated by maximizing the modified likelihood function

$$\mathcal{L}_T(\beta,\gamma) = \prod_{i=1}^{M} \frac{p(D_i;\beta,\gamma)}{1 - P(D_{\text{th}};\beta,\gamma)} \tag{18}$$

where D_{th} is the lower threshold under which the device is not able to detect the drops diameter; $P(D_i;\ \beta,\ \gamma)$ represents the cumulative distribution function (cdf). Similarly, the parameters of the probability distribution in the volume of air, $f_V(D)$, can be estimated by using the following expression

$$\mathcal{L}_T(\beta,\gamma) = \prod_{i=1}^{M} \left[\frac{p(D_i;\beta,\gamma)}{1 - P(D_{\text{th}};\beta,\gamma)}\right]^{N_i} \tag{19}$$

The term that appears at the denominator of Eqs. (18) and (19) is the degree of truncation, i.e. the mass of the probability

function that is not detected by the measurement device. Note that in the TML approach the total number of detected drops does not correspond exactly with n_c because small drops are not collected by the device.

3.3. Model testing and selection

Once the parameters of the three theoretical distributions are estimated by maximizing Eq. (12) or (13) (or Eqs. (18) and (19) following the truncated estimation approach, TML) we investigate the discrepancy between observed values and the values expected under the model in question by a goodness-of-fit test, which aims to justify whether the chosen distribution is acceptable or not. In this study, we adopt the Kolmogorov–Smirnov (KS) test (see e.g. Kottegoda and Rosso, 1997), which is based on the KS statistic that quantifies a distance between the empirical distribution function of the sample $\hat{F}(D)$ and the cumulative distribution function $F(D)$ of the reference distribution (namely gamma, lognormal or Weibull). In essence, the test does not reject the null hypothesis that the sample is drawn from the reference distribution with a significance level equal to α if the KS statistic, D_M, is

$$D_M < \Delta_M(\alpha) \tag{20}$$

where $\Delta_M(\alpha)$ is a critical reference value that decreases when increasing the sample size M and the significance level of the test α, and

$$D_M = \max_i \left| F(D_i) - \hat{F}(D_i) \right| \tag{21}$$

where $i = 1, \ldots, M$.

In this study the significance levels $\alpha = 0.01$ is used.

The empirical cdf is simply computed by sorting in ascending order the measured drop diameters and then using the common Weibull (plotting position) formula $\hat{F}(D_i) = i/(N+1)$, for the $f(D)$ fitting. Otherwise, in the case of the $f_V(D)$ fitting, we have (Adirosi et al., 2015)

$$\hat{F}_V(D_i) = \frac{1}{\sum_{z=1}^{M} 1/v(D_z)} \sum_{j=1}^{i} \frac{1}{v(D_j)} \tag{22}$$

When the TML estimates are tested, the measured diameter smaller than 0.2 mm are eliminated.

Since the parameters of the reference distributions are determined from the data (which means that we are testing the composite hypothesis that a sample of observations comes from a distribution whose parameters are unspecified), the critical values $\Delta_M(\alpha)$ of the KS test should be redetermined via Monte Carlo simulations for each sample and for each hypothetical distribution (see e.g. Kottegoda and Rosso, 1997; Laio, 2004). Indeed, the parameters of the theoretical cdfs are estimated from the same sample used in the test (as it is customary in hydrological applications); consequently, $\Delta_M(\alpha)$ is not independent on the hypothetical distribution $F(D)$. Moreover, $\Delta_M(\alpha)$ depends on the empirical cdf formula. Hence, $\Delta_M(\alpha)$ needs to be recalculated for each distribution model considered in our analysis, as described in the following. For each sample and for each distribution model, the Monte Carlo simulation consists in (i) generating a large number of samples from $F(D)$ (e.g. 1000), (ii) estimating the distribution parameters of each synthetic sample through maximum likelihood method (by Eq. (12) or (13) for the ML or Eq. (18) or (19) for TML), (ii) computing the corresponding value of the KS test statistics D_M following Eq. (21), and (iv) estimating $\Delta_M(\alpha)$ as the $(1-\alpha)$ quantile of the empirical distribution of D_M.

Since both D_M and $\Delta_M(\alpha)$ are peculiar of each sample and of each hypothetical distribution, their relative difference cannot be used to compare and rank the fitted distributions. To overcome this problem a "selection criterion" can be used to make a choice among the models that pass the KS test. The selection of the best model should deal with the trade-off between the model accuracy and the model complexity. To date, several selection criteria have been developed, such as the Akaike Information Criterion (AIC) and the Bayesian Information Criterion (BIC) (see e.g. Zucchini, 2000; Laio et al., 2009; Calenda et al., 2009). Both AIC and BIC reward model accuracy (as assessed by the likelihood function), but they also include a penalty term for the number of parameters.

As we consider only hypothetical distributions with the same number of parameters, the model selection is easily performed by comparing the maximized likelihood values.

4. Experimental data

In this study the drops spectra measured by 2D Video Disdrometers have been used. The 2DVD is an optical disdrometer that allows to measure the equivolumetric diameter (i.e. D) and fall velocity of each single hydrometeor that falls through its virtual measuring area of $10 \times 10\,\text{cm}^2$. The compact version of the 2DVD has two line-scan cameras with 632 pixel, a nominal resolution of about 0.16 mm; only the particles detected by both the cameras are analyzed by the 2DVD software.

In the last two decades, 2DVD has been employed in several field campaigns worldwide (Gatlin et al., 2015). The experimental data used in this study have been collected during four field campaigns around the globe. One dataset was collected during the first Special Observation Period (SOP1.1) of the HYdrological cycle in the Mediterranean EXperiment (HyMeX) field campaign in Rome, from September 2012 to November 2012 (Ferretti et al., 2014). The second dataset was collected during the Midlatitude Continental Convective Clouds Experiment (MC3E) in North Central Oklahoma from late April 2011 to early June 2011 (Jensen et al., 2015), and it consists of size spectra collected by five 2DVDs. The third dataset was collected by six different 2DVDs during the Iowa Flood Studies (IFloodS, http://iowafloodcenter.org/projects/ifloods/) field campaign in eastern Iowa from May 2013 to June 2013. Finally, the fourth dataset was collected more recently, from May 2014 to June 2014, during the Integrated Precipitation and Hydrology Experiment (IPHEx, http://iphex.pratt.duke.edu/node/50) in the southern Appalachian Mountains in the eastern United States by five 2DVDs. Three of those datasets (namely HyMeX, MC3E, and IFloodS) have been analyzed also in Adirosi et al. (2015).

All the datasets were pre-processed following the same procedure. As in other 2DVD related studies (Kruger and Krajewski, 2002; Thurai and Bringi, 2005; Jaffrain and Berne, 2011; Hauser, 1984; Tokay et al., 2001; Adirosi et al., 2015; Adirosi et al., 2014 among others), a filter criterion based on the fall velocity has been applied to each single drop in order to eliminate the spurious drops due to splashing, wind effects, or mismatching. We adopt herein the one of Tokay et al. (2001), which relies on the assumption that the law of Atlas et al. (1973) correctly describes the true relationship between the terminal velocity and the size of the drops; hence, it rejects the diameters whose measured velocity falls outside the range ±50% of the theoretical velocity law. We stress here that this kind of filter could accidentally remove some real raindrops together with the spurious ones, determining an error in the estimation of $f(D)$ and $f_V(D)$; yet, the investigation of such an effect goes beyond the scope of this work. For each dataset, the percentage of drops removed by the filtering is reported in Table 1 along with the number of 1-min drop spectra with at least 100 drops (used rain/no rain threshold), the mean and maximum values of the rain rate and maximum drop diameter (D_{max}), and the median value of sample size (M; namely the number of drops detected in 1 min). Note that most the drops removed by the filtering criterion are small to medium drops ($D \leq 2$ mm).

Table 1
Percentage of drops removed by the filtering criterion, i.e. drops that fall outside ±50% of the (7), number of selected 1-min samples, maximum and mean rain rate (R), maximum drop diameter (D_{max}), and sample size (M) for each dataset.

	% of filtered drops	# of 1-min samples	max(R) (mm h^{-1})	mean(R) (mm h^{-1})	max(D_{max}) (mm)	mean(D_{max}) (mm)	median(M)
HyMeX	14.2	2849	158.2	4.0	7.79	2.54	339
MC3E	11.3	6647	97.6	2.6	8.61	2.48	299
IFloodS	13.7	22, 125	195.2	2.6	9.18	2.26	378
IPHEx	14.2	10, 347	194.0	4.1	8.65	2.27	358

A quick and basic description of the four datasets has been provided by the plots of Fig. 2, that shows for each dataset the total number of drops measured in 1 min plotted versus *i)* D_{max} and *ii)* the value of mean diameter, D_{mean}. Data are presented in a two-dimensional density plots (namely 2D histograms) where the colorbar represents the percentage of occurrence in each cell. As expected, D_{max} increases with the number of detected drops. The minimum drop diameter collected by 2DVD are 0.18 mm, 0.12 mm, 0.18 mm and 0.17 mm for the HyMeX, IFloodS, IPHEx, and MC3E field campaigns respectively; these values are in agreement with the findings of Thurai et al. (2015). The biggest raindrop found in the four analyzed datasets has D equal to 9.18 mm; it belongs to the IFLoodS dataset and can be defined as a giant raindrop (namely a drop with $D > 8$ mm according to Gatlin et al. 2015). In total, there are 17 giant raindrops in the four 2DVD datasets considered in this study. Please note that the fall velocity filtering criterion adopted in this study allows to affirm that the particle analyzed are raindrops, although the latter giant drops could also belong to a rain-hail mixture (Gatlin et al., 2015). Most of the mean drop diameters are around 1 mm and their values are not significantly influenced by the total number of drops; in fact, when increasing M the mean diameter D_{mean} does not vary widely.

It is relevant to note that due to the natural ranges of rain drop dimensions, roughly between 0.1 mm (Pruppacher and Klett, 1997) and 9.7 mm (Gatlin et al., 2015), to the rounding effect (i.e. the equivolumetric diameter is recorded with two decimal places), and to the large amount of drops that can be recorded in 1 min (see Fig. 2), the available 2DVD measurements may be a discretized version of the actual continuous values of drop diameters. Fig. 3 shows the scatterplot of the number of detected drops against the percentages of repeated diameter (namely ties) of all the analyzed datasets (because they have similar behavior); the colors represent the corresponding value of D_{max}. From Fig. 3 it is evident that, fixing the number of detected drops, the percentage of ties increases when decreasing D_{max}. In order to remove the ties from our datasets, a randomization procedure commonly used in hydrology (see e.g. Chambers et al., 1983; Vanderberghe et al., 2010; Salvadori et al., 2014) has been applied to the data, by introducing a randomized diameter $\widetilde{D}_i$ as

$$\widetilde{D}_i = D_i + \varphi\, U_i \tag{23}$$

where $\varphi = 0.01$ mm is the rounding error and U_i is an independent identically distributed random variable uniform over the interval $(-0.5,\ 0.5)$ mm.

5. Results

The lognormal, Weibull and gamma distributions are fitted to the disdrometer-measured spectra under two different conditions, i.e. considering: (i) the probability distribution of drop diameter at ground, $f(D)$, and (ii) the more commonly used probability distribution of drop diameter per unit volume of air, $f_V(D)$. The parameters of the theoretical distributions, i.e. the scale (β) and the shape parameter (γ), are estimated using the ML method, based on Eqs. (12) and (13) for the fitting of $f(D)$ and $f_V(D)$ respectively. To estimate $f_V(D)$, the law of Atlas et al. (1973) was adopted, in agreement with the filtering criterion used to pre-process the data. Then the fitted distributions are tested by applying the KS test, Eqs. (20) and (21), respectively; the percentage of samples that pass the test (i.e. are not rejected) is defined as "pass rate" hereinafter. Finally, when more than one theoretical distributions pass the test, they are ranked according to their maximized log-likelihood, $\log\mathcal{L}(\beta, \gamma)$; in practice, the distribution that has the maximum log-likelihood value is the one that performs best. In the following, we call "success rate" the percentage of samples, among the ones that pass the KS test, that has been best fitted by a given theoretical model.

Table 2
Fitting of $f(D)$: percentage of 1-minute drop sample that a distribution passes (is not rejected) by the KS test at the $a = 1\%$ significance level for the datasets considered.

	Fitting of $f(D)$		
	gamma	lognormal	Weibull
HyMeX	31.0%	30.2%	18.4%
MC3E	33.8%	30.4%	21.6%
IFloodS	28.2%	20.0%	20.5%
IPHEx	33.0%	26.5%	22.0%

Furthermore, in order to investigate the effect of the lack of small drops (with $D < 0.2$ mm) due to instrumental limitations, the analyses were repeated by applying the truncated maximum likelihood approach based on Eqs. (18) and (19), where D_{th} is set equal to 0.2 mm. The truncated approach for parameter estimation was applied only to the HyMeX dataset.

Before presenting the overall results, we briefly discuss the effect of the presence of ties. In order to analyze the influence of ties on results, we apply the randomization procedure expressed by Eq. (23) to some selected samples of the HyMeX dataset. Specifically, we analyze results for some 1-min samples presenting different characteristics – in terms of length (M) and number of distributions that pass the KS test – in order to understand under which conditions the presence of ties might affect the results of our analysis. For each selected sample, we repeat the procedure presented in Section 3 for 300 times and compare the results (not shown) with those obtained for the original sample (not randomized) in terms of estimated parameters, log-likelihood values and results of the KS test. We find that the differences between the distribution parameters of the original sample and randomized ones are negligible. Most importantly, the results of the KS test for the original samples are the same as those of the randomized samples. Therefore, the analyses presented in this study are referred to the original measured datasets, without randomization.

5.1. Fitting of *f(D)*

Table 2 shows the KS test pass rates at level $\alpha = 0.01$ for the selected distributions. Although datasets are collected in four different regions, results are consistent with each other. The gamma distribution is the one that performs best with the lowest rejection rate ($\sim$ 68% on the average, considering the four datasets), while the Weibull distribution shows the highest rejection rate (

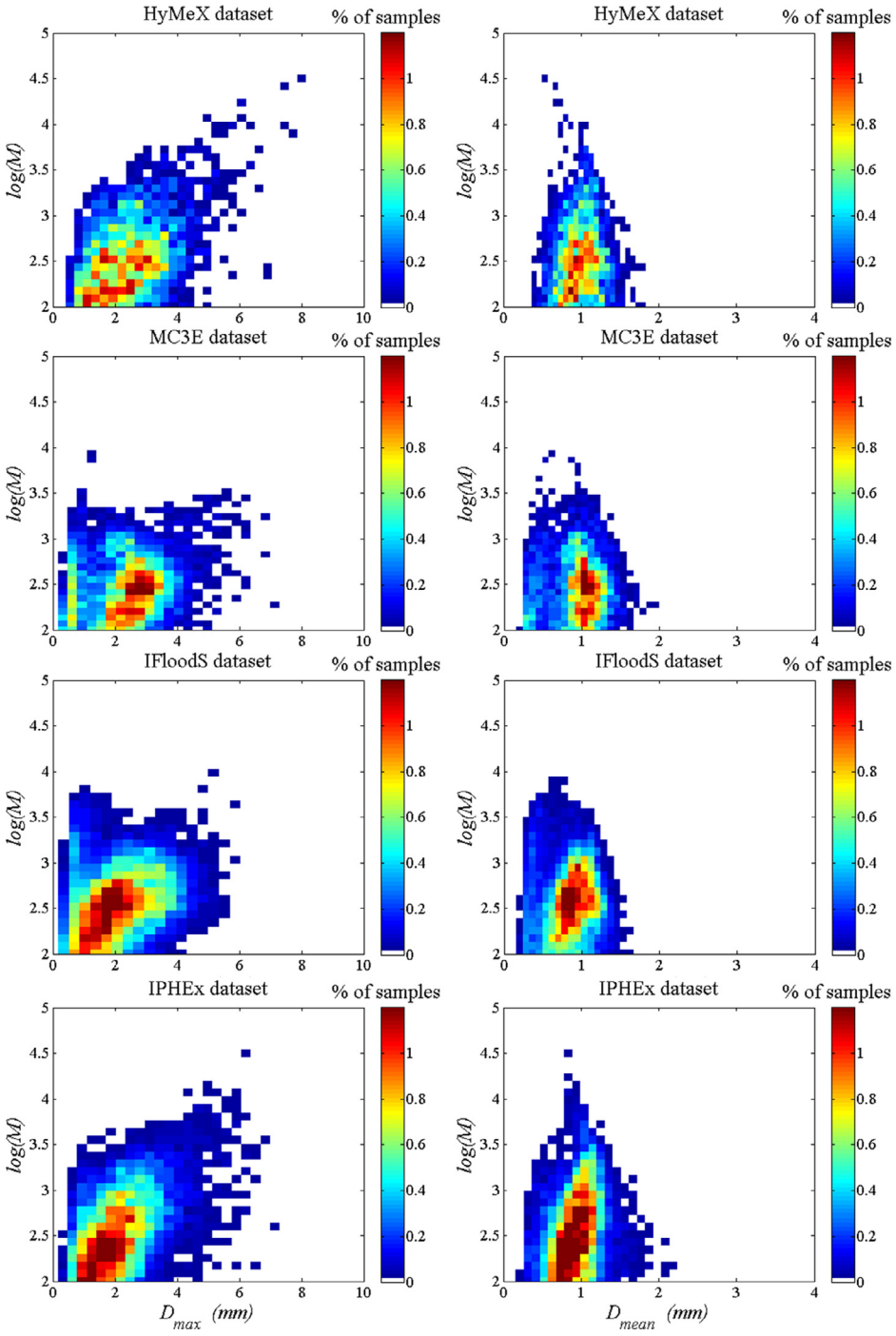

Fig. 2. For each dataset (row 1 for HyMeX, row 2 for MC3E, row 3 for IFloodS and row 4 for IPHEx) the number of drops detected in each minute is plotted versus (i) the maximum drop diameter (D_{max}; first column), and (ii) the mean drop diameter (D_{mean}; second column). The colorbar indicates the percentage of samples in each cell. (For interpretation of the references to colour in this figure legend, the reader is referred to the web version of this article.)

$\sim$ 79% on the average, considering the four datasets). The KS rejection rates are quite high, indicating that the selected theoretical distributions cannot adequately model all the empirical drop size distribution at the ground. The obtained rejection rates for the gamma and lognormal distribution are a bit higher than the ones obtained by Cugerone and De Michele (2015). This difference could be a consequence of the fact that while we analyze drop-by-drop data, Cugerone and De Michele (2015) used binned data (although a randomization procedure within the bin was applied) collected by a different type of disdrometer; further, the length of the measured drop spectra could have some influence, as discussed in the following. Finally, negligible variations of the values of the rejection rates are reached if the truncated approach for parameter estimation is considered (results not shown); further considerations on this issue are provided in the next section.

Considering only the distributions that pass the KS test, and selecting among them the one with the maximum values of log-likelihood (best fit), the gamma distribution results to be that with the highest percentage of success; however, such percentage is quite low being equal to $\sim$ 22% on average considering the four datasets (Table 3). As expected from the results in Table 2, for the majority of the samples no distribution fits properly the data; in

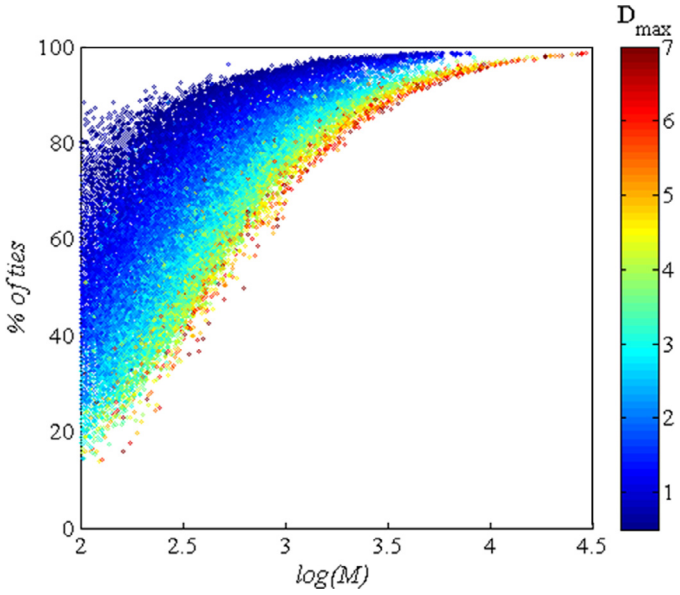

Fig. 3. Scatterplot between the number of detected drops in a given minute and the percentage of ties, as function of D_{max}. All the four datasets have been plotted together because they reveal the same behavior. (For interpretation of the references to colour in this figure legend, the reader is referred to the web version of this article).

Table 3
Fitting of $f(D)$: percentage of samples for which a model (gamma, lognormal or Weibull) is selected according to the log-likelihood criterion. The last column shows the percentage of samples that cannot be modelled by any of the considered distributions, according to the KS test at the $a = 1\%$ significance level for the datasets considered.

	Fitting of $f(D)$			
	gamma	lognormal.	Weibull	none
HyMeX	22.1%	14.3%	9.9%	53.6%
MC3E	22.0%	15.1%	11.6%	51.3%
IFloodS	21.0%	8.1%	12.2%	58.8%
IPHEx	22.8%	10.7%	13.8%	52.6%

Table 4
As Table 2 but for the fitting of $f_V(D)$.

	Fitting of $f_V(D)$		
	gamma	lognormal	Weibull
HyMeX	22.7%	18.7%	14.5%
MC3E	26.1%	21.1%	17.8%
IFloodS	16.3%	11.2%	14.1%
IPHEx	23.3%	17.7%	17.7%

other words, the KS test rejects all the distributions (last column of Table 3).

5.2. Fitting of $f_V(D)$

When directly fitting the probability distribution in the unit volume of air (Table 4), the rejection rates of the KS test are even higher for all of the reference distributions than those obtained when fitting $f(D)$. This difference is due to the velocity-diameter law of Atlas et al. (1973) used for $f_V(D)$ fitting, Eq. (7), which modifies the shape of $f_V(D)$ with respect to that of $f(D)$. As previously discussed in Section 2.2, the gamma shape of the distribution of the diameter in the unit volume of air, $f_V(D)$, is preserved into the distribution of the diameter at the ground, $f(D)$ (and vice-versa) when a power-law relationship between drops terminal velocity and diameter is adopted. This implies that when Eq. (6) is used for $f_V(D)$ estimation, we should have a rejection rate of the gamma distribution for $f_V(D)$ similar to that of $f(D)$. Hence, differences between the rejection rates reported in Tables 2 and 4 clearly indicate that the choice of the terminal fall velocity-diameter law has an impact on $f_V(D)$ assessment. This means that the absolute performance of a probability model in representing the natural variability of the DSD as measured by a disdrometer is conditioned on the functional form assumed for the velocity law.

Table 5
As Table 3 but for the fitting of $f_V(D)$.

	Fitting of $f_V(D)$			
	gamma	lognormal	Weibull	none
HyMeX	15.8%	10.7%	7.3%	66.2%
MC3E	16.7%	12.7%	8.6%	62.0%
IFloodS	11.5%	5.3%	8.6%	74.6%
IPHEx	16.0%	8.0%	11.1%	64.9%

The Weibull and the gamma distributions have the lowest and highest pass rate of KS test, respectively. Ranking the models according to their log-likelihood values (Table 5), we observe that for the HyMeX dataset about 16% of the measured drop spectra are best represented by a gamma distribution; such a percentage decreases to 11% and 7% of the data for the lognormal and Weibull distributions, respectively. For the other datasets the percentage of spectra best fitted by the Weibull distribution increases, mainly at the detriment of the lognormal distribution. These results are in quite good agreement with the findings of Adirosi et al. (2015).

Only for a small number of measured drop spectra (about 5% of the samples), all of the reference distributions pass the KS test, i.e. they are alternative model hypotheses. Fig. 4 shows for each dataset an example of 1-min spectra for which all the three distributions are alternative possible model; under this condition, the distribution that performs best has been selected comparing the values of the likelihood. By the maximum likelihood selection criterion, the distribution that performs best in such cases (that are a subsample of those considered in Table 5) is the gamma distribution. In Fig. 5 (first column) we show with different colors the number of times that the gamma (red), lognormal (green) and Weibull (blue) distributions have the best performance for all datasets.

To gain a deeper understanding, we evaluate the behavior of the candidate distributions in terms of other statistics that are not employed in the model fitting procedure. We use L-moments, because they are indeed useful summary statistics. These are analogous to the conventional moments but can be estimated by linear combinations of the elements of an ordered sample. L-moments have several advantages over conventional moments. For example, when estimated from a sample, they are more robust to the presence of outliers in the data. Moreover, the asymptotic efficiency of sample L-moments is less affected by heavy-tailed distributions than conventional moments (Lombardo et al., 2014). Another advantage is that their existence only requires the random variable to have finite mean, so the L-moments exist even if the higher conventional moments do not exist (Hosking and Wallis, 1997). We consider herein L-moments with orders ranging from one to four. The first L-moment (ℓ_1) directly corresponds to the mean; the others (ℓ_{2-4}) can be computed as linear combinations of the probability weighted moments (b_k) as $\ell_2 = 2\ b_1 - \ b_0$, $\ell_3 = 6\ b_2 - 6\ b_1 + \ b_0$ and $\ell_4 = 20\ b_3 - 30\ b_2 + 12\ b_1 - \ b_0$. Then, we derive and compare the theoretical and empirical L-moments for all the candidate distributions in order to assess which performs best.

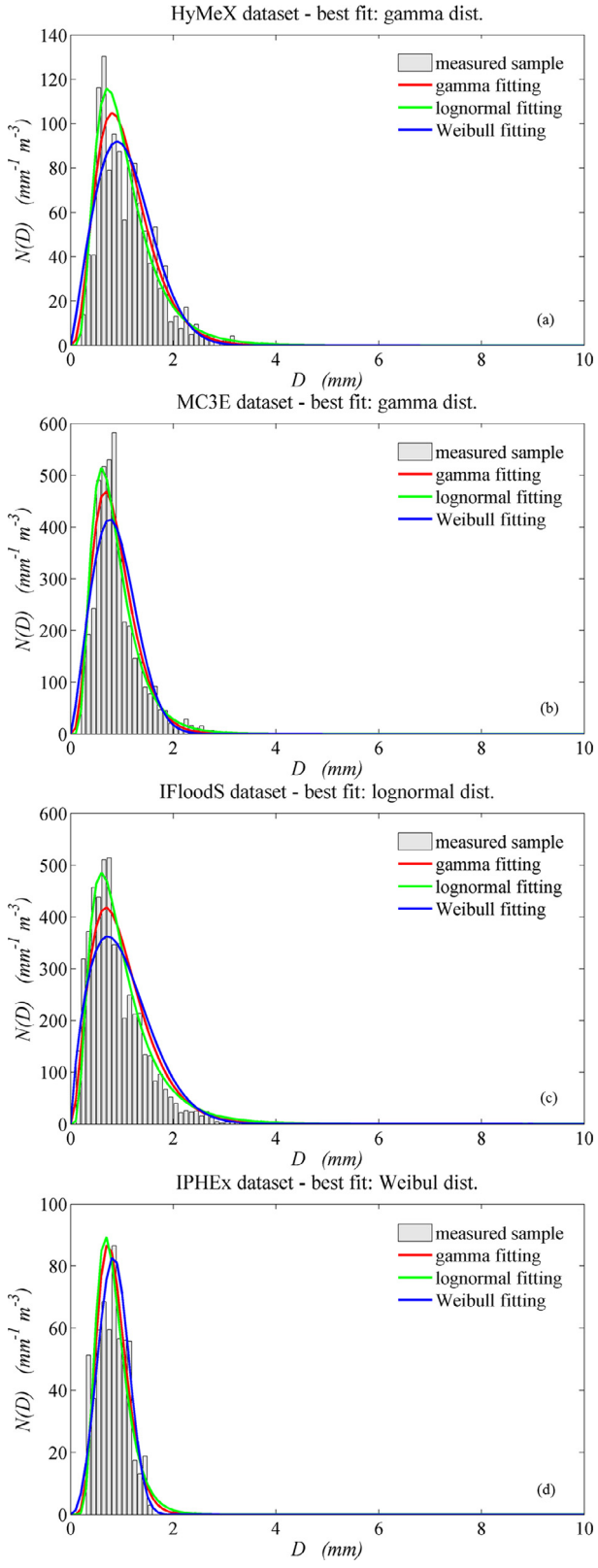

Fig. 4. For each dataset an example of measured 1-minute sample has been provided (grey bars) along with the three fitted distributions: gamma (red line), lognormal (green line) and Weibull (blue line). For the four depicted samples, all of the reference distributions pass the KS test, and the one that preforms best according to the likelihood criterion has been reported in the title of each plot. (For interpretation of the references to colour in this figure legend, the reader is referred to the web version of this article.)

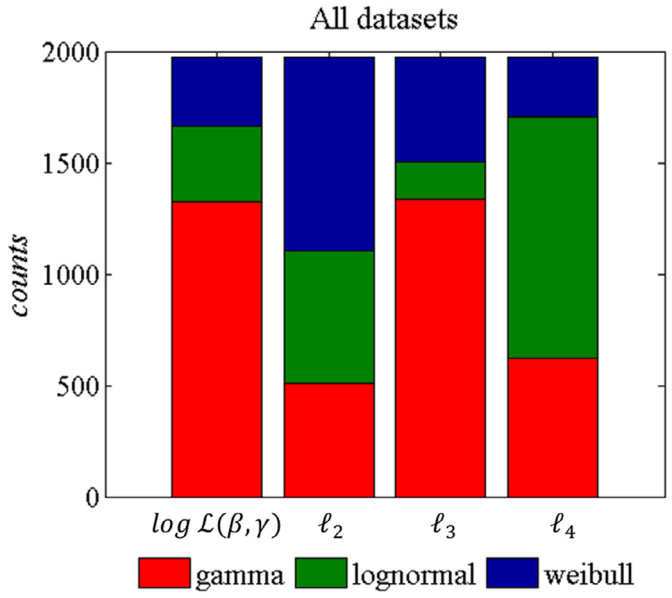

Fig. 5. Each column shows the number of empirical drop spectra that can be represented by the three theoretical distributions considered in this study. The colors depict the number of samples for which the gamma (red), lognormal (green) or Weibull (blue) distribution has the maximum values of log-likelihood, $\log\mathcal{L}(\beta,\gamma)$ (first column) or the minimum difference between the sample and theoretical L-moments, ℓ_2 (second column), ℓ_3 (third column), and ℓ_4 (fourth column). (For interpretation of the references to colour in this figure legend, the reader is referred to the web version of this article.)

The theoretical probability weighted moments b_k can be computed as (Hosking, 1990)

$$b_k = \int D\, f_V(D)\, [F_V(D)]^k dD \tag{24}$$

where $f_V(D)$ and $F_V(D)$ are the pdf and cdf of drop diameters per unit volume of air, respectively, of each model with parameters estimated by maximum likelihood method (Section 3.2). The sample moments ($\hat{b}_k$) can be computed as

$$\hat{b}_k = \sum_{i=1}^{M} D_i\, \hat{f}_V(D_i)\, \left[\hat{F}_V(D_i)\right]^k \tag{25}$$

where $\hat{F}_V(D_i)$ is given by (22) and, as a consequence, the corresponding pdf is given by $\hat{f}_V(D_i) = \frac{1/v(D_i)}{\sum_{z=1}^{M} 1/v(D_z)}$. Substituting the latter expression and Eq. (22) in Eq. (25) we obtain

$$b_k = \sum_{i=1}^{M} D_i\, \frac{v(D_i)^{-1}}{\sum_{z=1}^{M} v(D_z)^{-1}} \left[\frac{\sum_{j=1}^{i} v(D_j)^{-1}}{\sum_{z=1}^{M} v(D_z)^{-1}}\right]^k \tag{26}$$

The comparison between theoretical and sample L-moments shows a very good agreement for ℓ_1 and ℓ_2, while a larger dispersion is present for the higher order L-moments (not shown). Indeed, we recall here that the maximum likelihood method used for parameter estimation is grounded on the concept of selecting the model that best describes the bulk of the empirical distribution, which is accounted for by the low order moments (ℓ_1 and ℓ_2 in the case of L-moments).

If we rank the candidate models according to the minimum absolute error between theoretical and empirical L-moments (last three columns of Fig. 5), the number of times that a certain model performs best might change with respect to that obtained following the maximum likelihood selection criterion. Note that results for ℓ_1 are not shown because the maximum likelihood method implies that the theoretical mean equals the sample mean for the

Table 6
Distribution of the number (#) of HyMeX samples with the samples size (M) and the percentages of these samples that can be represented by the gamma, lognormal and Weibull distribution or by none of them.

	HyMeX				
	#	gamma	lognormal	weibull	none
$M \leq 200$	777	44.62%	41.50%	30.61%	39.6%
$200 < M \leq 500$	1115	24.55%	17.90%	13.85%	61.4%
$500 < M \leq 1000$	537	5.21%	2.61%	3.35%	89.8%
$1000 < M \leq 2500$	344	0.58%	0%	1.45%	98.0%
$M > 2500$	76	0%	0%	0%	100%

Table 7
Percentage of samples that cannot be represented by any of the three models analyzed in this study, for MC3E, IFloods and IPHEx datasets and for different sample sizes (M).

	MC3E	IFloodS	IPHEx
$M \leq 200$	41.9%	52.0%	39.5%
$200 < M \leq 500$	59.8%	69.2%	56.1%
$500 < M \leq 1000$	85.9%	91.0%	83.8%
$1000 < M \leq 2500$	98.6%	99.0%	98.2%
$M > 2500$	100%	100%	100%

gamma distribution (Marzuki et al., 2012); in other words, since ℓ_1 is the mean and the gamma parameters have been estimated by maximum likelihood method, by definition the gamma distribution will always be the best model if we assess the relative quality of models by ℓ_1. Results summarized in Fig. 5 suggest that the selection criterion might influence the choice of the best distribution. Specifically, the lognormal distribution could be selected as the best one if we look at the performance of the model in terms of the higher order moment (compare Adirosi et al., 2015). Since L-moments are essentially linear moments, although probability weighted, as the likelihood they are influenced by the bulk of the distribution. It means that we may expect even more contrasting results in the case the raw moments (instead of the L-moments) are used; however, due to the strong uncertainty that specifically characterizes the high order moments (≥ 3), results would be of difficult interpretation.

The use of a truncated approach for $f_V(D)$ parameter estimation (TML, Eq. (19)) gives similar results with respect to those obtained by the complete maximum likelihood (ML) approach in terms of both the parameter values (Fig. 6) and the KS test pass rate. As an example, Fig. 6 depicts the scatterplot between the distribution parameters retrieved through complete (ML) and truncated (TML) methods in the cases the distributions estimated with both the methods are not rejected by the KS test. The figure shows that the estimated parameters do not vary much when using the truncated approach instead of the complete one. As for the KS test, the pass rate only slightly increases for all the distributions (results not shown).

While the selected models represent good alternative hypotheses for some samples, last column of Table 5 shows that ~65% of the drop spectra measured during all the field campaigns cannot be represented by any of the three models considered in this study. As previously stated, the presence of ties as well as the inability of the 2DVD to correctly detect the small drops ($D < 0.2$ mm) are not sufficient to explain the fact that a distribution cannot be represented by any of the three tested models. Yet, this high rejection rate can be justified by the large sample size, M. As shown in Table 6 for the HyMeX dataset, most of the drop spectra have a relatively low number of drops ($M < 500$), but, also many large samples ($M > 1000$) are present (column 2). If we look at the percentage of samples for which none of the distributions passes the KS test (Table 6, last column), it is ~ 40% for small sample sizes, while it tends to 100% when increasing M. Similar results are summarized in Table 7 for the other datasets. We can also notice from Table 6 (columns 3–5) that for small samples the pass rate of each distribution approaches that already obtained by Cugerone and De Michele (2015) for $f(D)$. Therefore, for the larger samples we can argue that all the distributions are rejected because the KS test becomes more and more strict for increasing M. More complex distributions (e.g. with a higher number of parameters, such as the one used by Cugerone and De Michele, 2015) could be able to represent these large samples, being supported by statistical goodness-of-fit tests, but, as explained in Section 1, distributions with more than two parameters are hardly retrievable due to the limited number of independent measurements available to common rainfall remote sensing techniques.

Finally, we show in Figs. 7 and 8 the frequency distributions of the scale and shape parameters of the best models (according to the log-likelihood criterion) for the four datasets. Although the four datasets have been collected in four different regions, the distributions of the fitted parameters are similar to each other. Moreover, their values are in good agreement with those shown by Adirosi et al. (2015), who directly fit and compare the models to data records by a simple and straightforward method. Interestingly enough, when the Weibull distribution is the best model, its shape parameter is always greater than one (see Fig. 8), thus indicating that the distribution has a very light tail, i.e. the tail approaches zero more rapidly than an exponential tail (Teugels, 1975). Similar considerations apply to the gamma distribution; in fact, the retrieved gamma shape parameters are always greater than one, which means that the gamma distribution never degenerates in the exponential one. This is true also in the case the truncated maximum likelihood approach is used for parameter estimation (see Fig. 6).

5.3. Practical implications

In Section 5.2, we show how well some widely used distributions fit the raindrop spectra measured by the two-dimensional video disdrometers, which are the most accurate drop sampling devices available nowadays. We develop our study by providing corroborating evidence from analyses of several record raindrop sizes in four different regions worldwide. However, one of the most useful and challenging issue related to the modelling of the natural DSD is to define "when" the assumption of the given distribution is valid or not; i.e. under which conditions it is preferable to represent the natural DSD by a given functional form. This information can be extremely helpful in the development of precipitation retrieval algorithms from remote sensing measurements or numerical weather prediction models.

In order to shed some light on this important issue, we investigate the behavior of some parameters directly obtained from measured DSD with respect to the distribution that best models the data. For a given minute, the best model is the one, among the distributions that pass the KS test, that provides the maximum value of likelihood. The selected dependent variables are the maximum drop diameter (D_{max}), the total number of detected drops (M), the percentage of small ($D < 1$ mm) and midsize ($1 < D < 3$ mm) drops, the rain rate (R) and the raindrop mass spectrum mean diameter (D_{mass}). Such variables are indeed commonly used to characterize the natural DSD in the literature, because, for instance, they are directly related to different physical processes occurring during the formation and evolution of the precipitation such as coalescence, break-up, accretion and evaporation (Rosenfeld and Ulbrich, 2003), and can be used to classify the different precipitation types.

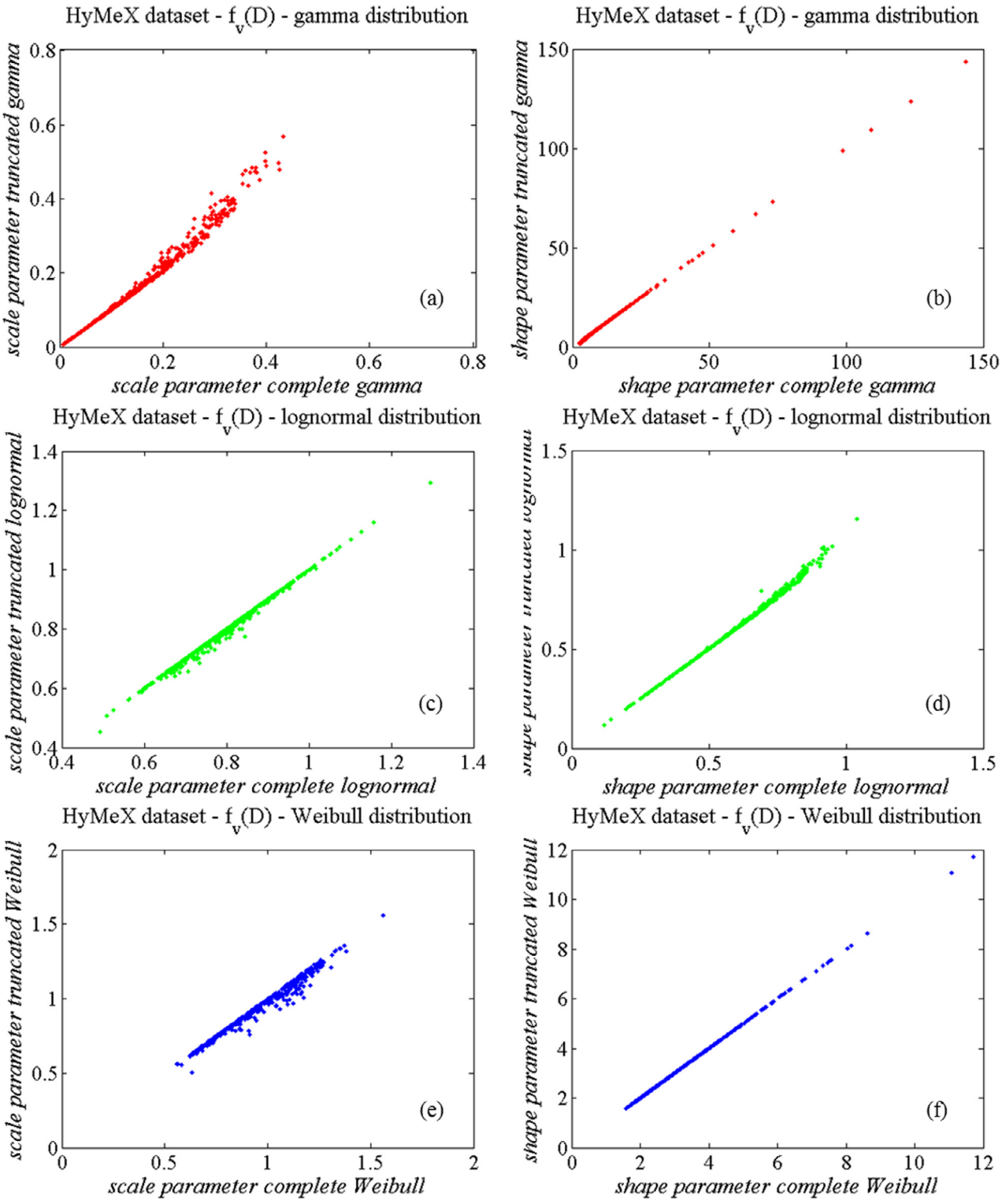

Fig. 6. Scatterplot between the distribution parameters retrieved through complete and truncated ML method in the cases the distributions estimated with both the methods are not rejected by the KS test.

We recall here that the rain rate can be directly obtained from disdrometer DSD as

$$R = 6\ \pi\ 10^{-4} \int_{D_{min}}^{D_{max}} v(D)N(D)D^3\ dD\ \left(mm\ h^{-1}\right) \tag{27}$$

while D_{mass} can be obtained as the ratio of the fourth and third moment of the drop size distribution and it is one of the three parameters of the normalized gamma distribution (Testud et al., 2001) often employed to estimate the DSD parameters (Bringi et al., 2002 among others). From a physical point of view, D_{mass} is the first moment of the mass spectrum that represents the mass of liquid water as a function of the drop diameter (Williams et al., 2014) and is correlated to the percentage of large drops and to D_{max}. In fact, for a given rain rate, higher D_{mass} corresponds to a spectrum with larger drops (Tokay et al., 2001).

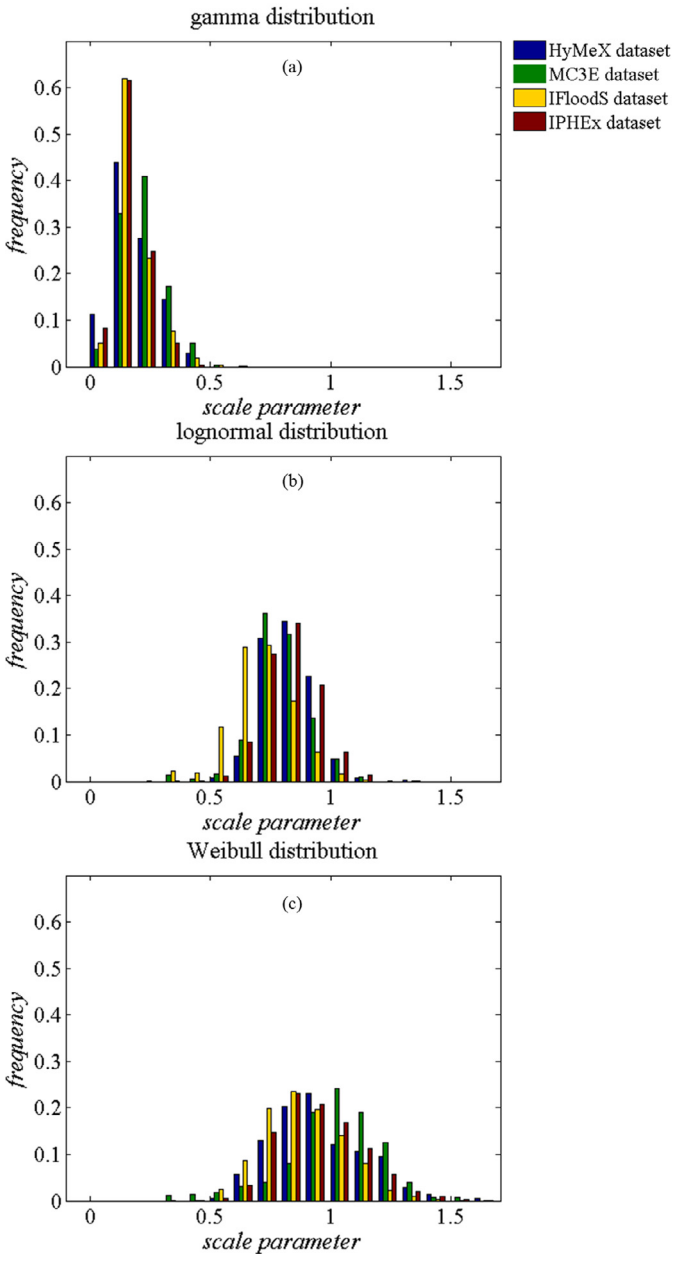

Fig. 7. Distribution of the scale parameter for all the minutes best fitted by the (a) gamma, (b) lognormal and (c) Weibull distribution, for each dataset taking into accounts only the distributions that pass the test. (For interpretation of the references to colour in this figure legend, the reader is referred to the web version of this article).

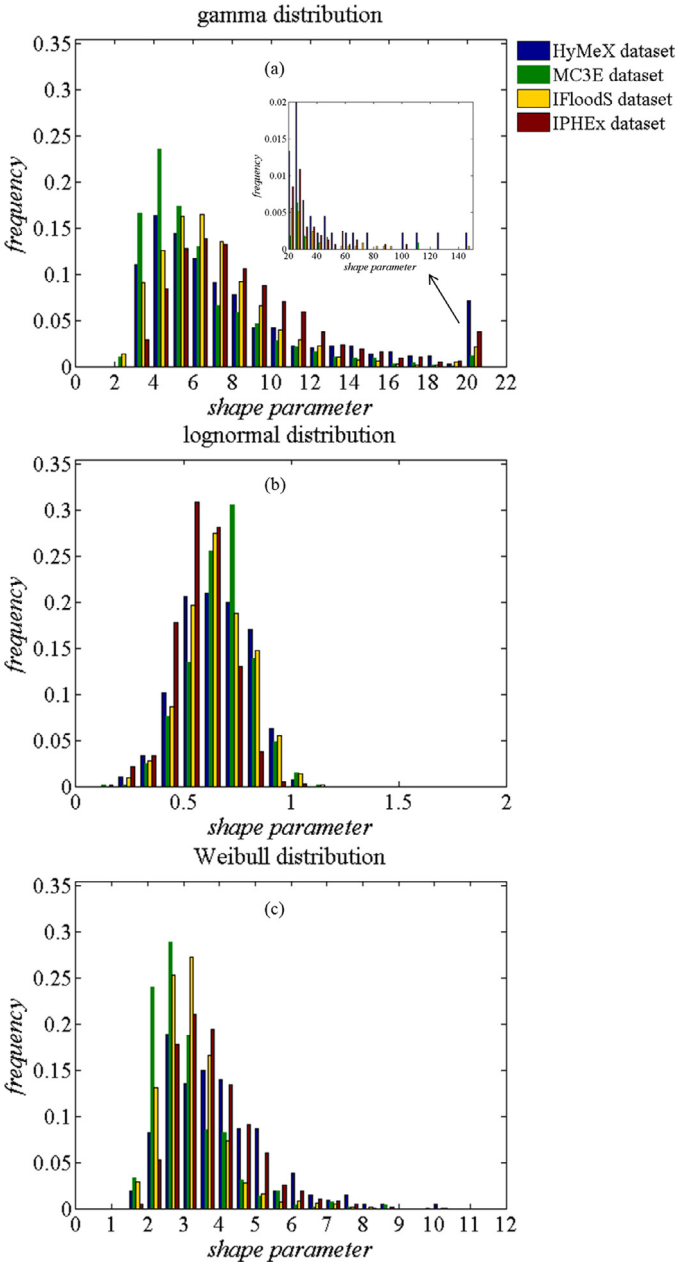

Fig. 8. As Fig. 7 but for the shape parameters. For the gamma distribution a small plots shows the distribution of the shape parameters greater than 20. (For interpretation of the references to colour in this figure legend, the reader is referred to the web version of this article).

In Fig. 9 the pdfs of the dependent variables are plotted for the drop spectra best fitted by the gamma distribution (red lines), the lognormal distribution (green lines) and the Weibull distribution (blue lines) respectively. For brevity, the results are shown only for the HyMeX dataset, since similar conclusions can be drawn for the other datasets. We also show in Fig. 9 the pdfs of the dependent variables for the samples that are not represented by any of the probability models (black lines).

Fig. 9a shows that if the Weibull distribution (i.e. a light-tailed distribution) has the best fit (i.e. the maximum likelihood value), then the maximum diameters of the corresponding samples are generally lower than those of the samples that are best represented by the lognormal or gamma distributions. In fact, the corresponding pdf (blue line of Fig. 9a) is shifted toward lower diameters (for HyMeX the mode corresponds to $D_{max} \cong 1.5$ mm). The opposite reasoning holds for the lognormal model, which is indeed a heavy-tailed distribution. Therefore, it can be argued that if drop spectra spread out over a wide range of diameters, then it is likely that the lognormal distribution fits better the data. Conversely, narrower drop spectra tend to be better modelled by a Weibull distribution.

On the other hand, it seems that the sample size does not affect the selection of the best model (Fig. 9b). Note that we restrict our analyses to samples with at least 100 drops. Considering the percentage of small and midsize drops, we can claim that if the sample is mainly composed of small drops ($D < 1$ mm), then the Weibull distribution is more likely to best fit the data (Fig. 9c). By contrast, if midsize drops are more frequent in the sample, then the lognormal and the gamma models are favorites (Fig. 9d).

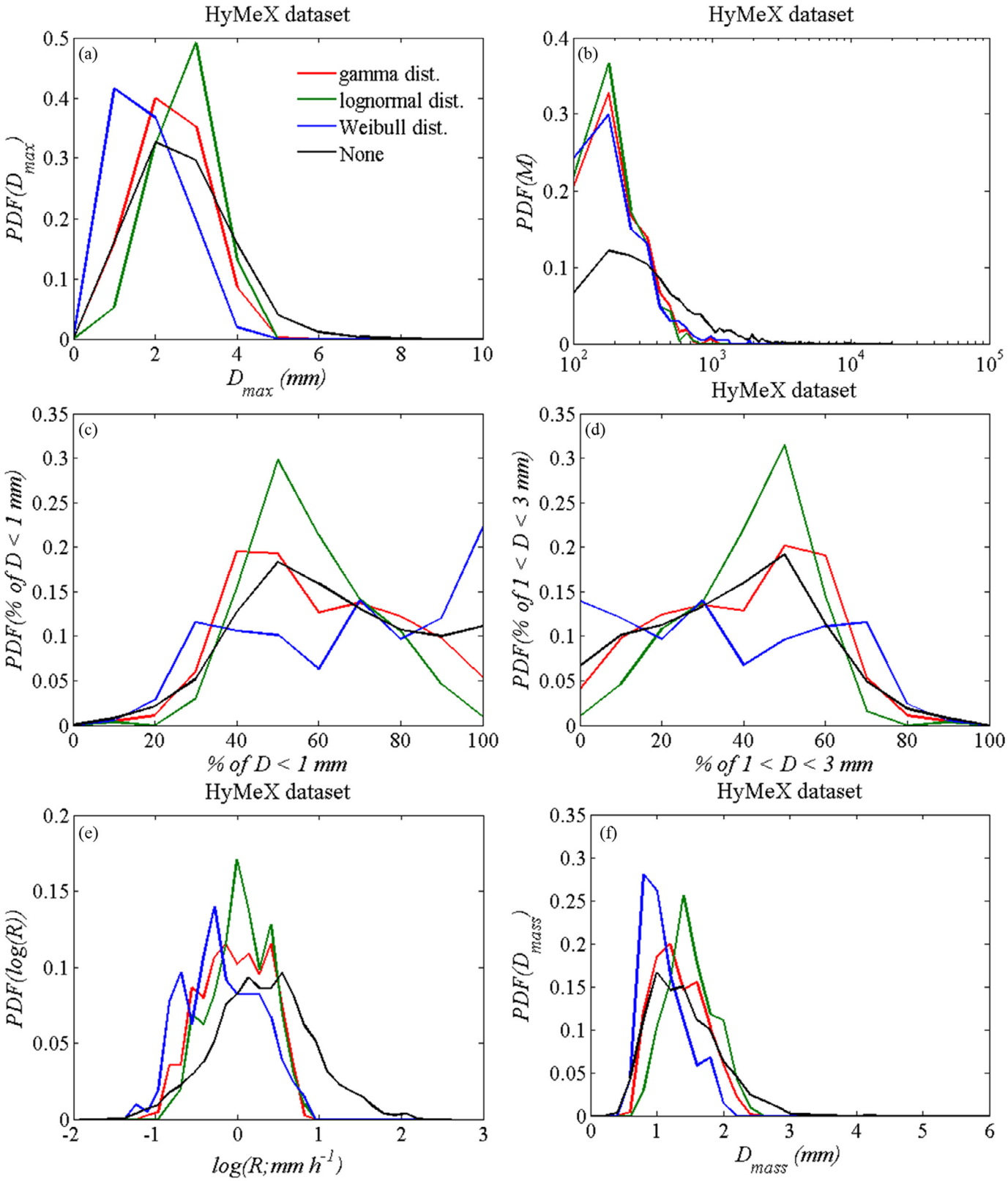

Fig. 9. Pdfs of (a) the maximum drop diameter (D_{max}), (b) the total number of detected drops (M), (c) the percentage of small ($D < 1$ mm) and (d) midsize ($1 < D < 3$ mm) drops, (e) rain rate (R) and (f) raindrop mass spectrum mean diameter (D_{mass}) for each minute of the HyMex dataset best fitted by the gamma (red lines), the lognormal (green lines) and the Weibull distribution (blue lines), or by any of the latter three distributions (black lines). (For interpretation of the references to colour in this figure legend, the reader is referred to the web version of this article).

In Fig. 9e, the pdfs of the retrieved rain rate from the samples best fitted by gamma, lognormal and Weibull distributions are plotted. Again, the Weibull distribution fits best the samples characterized by a low rain rate ($R < 1\,\mathrm{mm\,h^{-1}}$), while the other two models fit well the remainder. Finally, we show the behavior of D_{mass} in Fig. 9f. Samples with higher D_{mass} (with mean equal to 1.76 mm) – i.e. samples with a greater number of large drops – seem to be better fitted by a lognormal distribution. The samples with a lower D_{mass} (with mean equal to 1.11 mm) are best modelled by a Weibull distribution, while the samples best represented by a gamma distribution have a mean value of D_{mass} equal to 1.34 mm.

Results shown in Fig. 9 indicate that a heavy-tailed distribution (i.e. the lognormal model) is more appropriate to represent the variability of drop sizes in the presence of high rainfall rates and large drops. This has a strong practical implication, since the departure from a light-tail behavior may imply a dramatic increase of uncertainty in the statistical estimation of high-order DSD moments, as already discussed in detail in Adirosi et al. (2015). For even larger rain rates (Fig. 9e) and amount of large drops (Fig. 9a), and more generally of collected drops (Fig. 9b), the measured drop spectra cannot be statistically represented by any of the three models considered in this study (black lines).

6. Conclusions

The raindrop size distribution can be expressed as the product of the concentration of the raindrops and the probability distribution of drop sizes in a volume of air. The former can be directly obtained from disdrometer data by calculating the zeroth moment of the DSD, while determining the latter is the focus of this paper.

As follow-up of Adirosi et al. (2015), in this study three well known and widely adopted theoretical distributions (namely gamma, lognormal and Weibull) have been fitted to almost 42.000 1-minute drop spectra measured by two-dimensional video disdrometers. The main purpose of this work is to assess how often and how good the most commonly used models fit the empirical data, searching for the conditions under which each model performs best.

In order to achieve such an objective, we follow an up-to-date statistical approach based on the maximum likelihood fitting method and the Kolmogorov–Smirnov goodness-of-fit test. Furthermore, we carry out two different fitting procedures by using (i) the probability distribution of drop diameters at ground, and (ii) the more commonly used probability distribution of drop diameters per unit volume. The availability of large drop-by-drop datasets from four different regions in USA and Italy has allowed us to perform a robust statistical analysis whose findings are not site-specific. The main conclusions drawn in this work are summarized in the following.

In general, the gamma, lognormal and Weibull distributions are appropriate models to represent the distribution of drop diameters both at the ground and per unit volume of air; however, those distributions are adequately supported by statistical goodness-of-fit tests only for limited samples sizes. The discrepancy between the DSD and the drop distribution at the ground is due the effect of the size-fall velocity relation adopted to obtain the DSD, as pointed out in Section 2.2.

The Gamma distribution is ranked as first in fitting the data records, thus indicating that the probability distributions whose tails are exponentially bounded, i.e. light-tailed distributions, seem to be adequate to model the natural variability of DSDs. However, the lognormal distribution is the best model in a significant number of cases. The analysis of some dependent variables related to the DSD suggests that the lognormal distribution best represents the samples characterized by high values of the maximum diameter (D_{max}), rainfall rate (R) and raindrop mass spectrum mean diameter (D_{mass}). While the opposite is generally valid for the Weibull distribution. Hence, in line with our previous study, the frequency distributions of empirical DSDs can be heavy-tailed, thus potentially yielding a severe uncertainty in estimating statistical moments and bulk variables.

Finally, it is worth noting that in $\sim$ 60% of the samples the use of the distributions considered in this work is not statistically supported by the KS goodness-of-fit test; such an issue is directly related to the sample size, but not to the instrumental limitations for small drop size, or to the percentage of ties. The clear identification of the reasons for this behavior and the analysis of alternative 2-parameter models deserve further investigations that we leave for future works.

Acknowledgements

All authors acknowledge the International Cooperation of the Ground Validation program of the GPM mission. E. Adirosi and L. Baldini acknowledge the support of the Italian Civil Protection Department.

References

Adirosi, E., Gorgucci, E., Baldini, L., Tokay, A., 2014. Evaluation of gamma raindrop size distribution assumption through comparison of rain rates of measured and radar-equivalent gamma DSD. J. Appl. Meteorol. Clim. 53, 1618–1635. http://dx.doi.org/10.1175/JAMC-D-13-0150.1.

Adirosi, E., Baldini, L., Lombardo, F., Russo, F., Napolitano, F., Volpi, E., Tokay, A., 2015. Comparison of different fittings of drop spectra for rainfall retrievals. Adv. Water Resour. 83, 55–67. http://dx.doi.org/10.1016/j.advwatres.2015.05.009.

Adirosi, E., Baldini, L., Roberto, N., Gatlin, P., Tokay, A., 2016. Vertical profiles of raindrop size distribution using micro rain radar and 2D video disdrometer measurements. Atmos. Res. 169, 404–415. http://dx.doi.org/10.1016/j.atmosres.2015.07.002.

Angulo-Martínez, M., Barros, A.P., 2015. Measurement uncertainty in rainfall kinetic energy and intensity relationships for soil erosion studies: an evaluation using PARSIVEL disdrometers in the Southern Appalachian mountains. Geomorphology 228, 28–40. http://dx.doi.org/10.1016/j.geomorph.2014.07.036.

Atlas, D., Srivastava, R.C., Sekhon, R.S., 1973. Doppler radar characteristics of precipitation at vertical incidence. Rev. Geophys. 11, 1–35. http://dx.doi.org/10.1029/RG011i001p00001.

Atlas, D., Ulbrich, C.W., 1977. Path-and area-integrated rainfall measurement by microwave attenuation in the 1-3 cm band. J. Appl. Meteorol. 16, 1322–1331. http://dx.doi.org/10.1175/1520-0450(1977)016⟨1322:PAAIRM⟩2.0.CO;2.

Awang, M.A., Din, J., 2004. Comparison of the rain drop size distribution model in tropical region. In: RF and Microwave Conference, 2004. RFM 2004. Proceedings. IEEE 2004.

Beard, K.V., Pruppacher, H.R., 1969. A determination of the terminal velocity and drag of small water drops by means of a wind tunnel. J. Atmos. Sci. 26, 1066–1072. http://dx.doi.org/10.1175/1520-0469(1969)026⟨1066:ADOTTV⟩2.0.CO;2.

Beard, K.V., 1976. Terminal velocity and shape of cloud and precipitation drops aloft. J. Atmos. Sci. 33, 851–864. http://dx.doi.org/10.1175/1520-0469(1976)033⟨0851:TVASOC⟩2.0.CO;2.

Beard, K.V., 1985. Simple altitude adjustments to raindrop velocities for Doppler radar analysis. J. Atmos. Oceanic Technol. 2, 468–471. http://dx.doi.org/10.1175/1520-0426(1985)002⟨0468:SAATRV⟩2.0.CO;2.

Brandes, E.A., Vivekanandan, J., Wilson, J.W., 1999. A comparison of radar reflectivity estimates of rainfall from collocated radars. J. Atmos. Ocean. Tec. 16, 1264–1272. http://dx.doi.org/10.1175/1520-0426(1999)016⟨1264:ACORRE⟩2.0.CO;2.

Brandes, E.A., Zhang, G., Vivekanandan, J., 2002. Experiments in rainfall estimation with a polarimetric radar in a subtropical environment. J. Appl. Meteor. 41, 674–685. http://dx.doi.org/10.1175/1520-0450(2002)041⟨0674:EIREWA⟩2.0.CO;2.

Bringi, V.N., Huang, G.-J., Chandrasekar, V., Gorgucci, E., 2002. A methodology for estimating the parameters of a gamma raindrop size distribution model from polarimetric radar data: application to a squall-line event from the TRMM/Brazil campaign. J. Atmos. Oceanic Technol. 19, 633–645. http://dx.doi.org/10.1175/1520-0426(2002)019⟨0633:AMFETP⟩2.0.CO;2.

Brown, B.R., Bell, M.M., Frambach, A.J., 2016. Validation of simulated hurricane drop size distributions using polarimetric radar. Geophys. Res. Lett. 43, 910–917. http://dx.doi.org/10.1002/2015GL067278.

Calenda, G., Mancini, C.P., Volpi, E., 2009. Selection of the probabilistic model of extreme floods: the case of the River Tiber in Rome. J. Hydrol. 371, 1–11. http://dx.doi.org/10.1016/j.jhydrol.2009.03.010.

Caracciolo, C., Prodi, F., Battaglia, A., Porcu', F., 2006. Analysis of the moments and parameters of a gamma DSD to infer precipitation properties: a convective stratiform discrimination algorithm. Atmos. Res. 80, 165–186. http://dx.doi.org/10.1016/j.atmosres.2005.07.003.

Chambers, J.M., Cleveland, W.S., Kleiner, B., Tukey, P., 1983. Graphical Methods for Data Analysis. Wadsworth International Group, California.

Cugerone, K., De Michele, C., 2015. Johnson SB as general functional form for raindrop size distribution. Water Resour. Res. 51, 6276–6289. http://dx.doi.org/10.1002/2014WR016484.

D'Adderio, L.P., Porcù, F., Tokay, A., 2015. Identification and analysis of collisional breakup in natural rain. J. Atmos. Sci. 72, 3404–3416. doi: http://dx.doi.org/10.1175/JAS-D-14-0304.1 .

Ekerete, K.'u.-M.E., Hunt, F.H., Jeffery, J.L., Otung, I.E., 2015. Modeling rainfall drop size distribution in southern England using a Gaussian mixture model. Radio Sci 50. http://dx.doi.org/10.1002/2015RS005674.

Ferretti, R., Pichelli, E., Gentile, S., Maiello, I., Cimini, D., Davolio, S., et al., 2014. Overview of the first HyMeX special observation period over Italy: observations and model results. Hydrol. Earth Syst. Sci. 18, 1953–1977. http://dx.doi.org/10.5194/hess-18-1953-2014.

Gatlin, P.N., Thurai, M., Bringi, V.N., Petersen, W., Wolff, D., Tokay, A., et al., 2015. Searching for large raindrops: a global summary of two-dimensional video disdrometer observations. J. Appl. Meteor. Climatol. 54, 1069–1089. http://dx.doi.org/10.1175/JAMC-D-14-0089.1.

Gunn, R., Kinzer, G.D, 1949. The terminal velocity of fall for water droplets in stagnant air. J. Meteorol. 6, 243–248. http://dx.doi.org/10.1175/1520-0469(1949)006⟨0243:TTVOFF⟩2.0.CO;2.

Haddad, Z.S., Durden, S.L., Im, E., 1996. Parameterizing the raindrop size distribution. J. Appl. Meteor. 35, 3–13. http://dx.doi.org/10.1175/1520-0450(1996)035⟨0003:PTRSD⟩2.0.CO;2.

Hauser, D., Amayenc, P., Nutten, B., Waldteufel, P., 1984. A new optical instrument for simultaneous measurement of raindrop diameter and fall speed distributions. J. Atmos. Oceanic Technol. 1, 256–269. http://dx.doi.org/10.1175/1520-0426(1984)001⟨0256:ANOIFS⟩2.0.CO;2.

Hosking, R.M., Wallis, J.R, 1997. Regional Frequency Analysis: An Approach Based on L-Moments. Cambridge University Press, Cambridge, UK, p. 224.

Hosking, J.R.M., 1990. L-moments: analysis and estimation of distributions using linear combinations of order statistics. J. R. Stat. Soc. Ser. B 52, 105–124.

Hou, A.Y., Kakar, R.K., Neeck, S., Azarbarzin, A.A., Kummerow, C.D., Kojima, M., et al., 2014. The global precipitation measurement mission. Bull. Amer. Meteor. Soc. 95, 701–722. http://dx.doi.org/10.1175/BAMS-D-13-00164.1.

Ignaccolo, M., De Michele, C., 2014. Phase space parameterization of rain: the inadequacy of gamma distribution. J. Appl. Meteorol. Clim. 53, 548–562. http://dx.doi.org/10.1175/JAMC-D-13-050.1.

Jaffrain, J., Berne, A., 2011. Experimental quantification of the sampling uncertainty associated with measurements from PARSIVEL disdrometers. J. Hydrometeor 12, 352–370. http://dx.doi.org/10.1175/2010JHM1244.1.

Jameson, A.R., Larsen, M.L., 2016. The variability of the rainfall rate as a function of area. J. Geophys. Res. Atmos. 121, 746–758. http://dx.doi.org/10.1002/2015JD024126.

Jensen, M.P., Petersen, W.A., Bansemer, A., Bharadwaj, N., Carey, L.D., Cecil, D.J., et al., 2015. The midlatitude continental convective clouds experiment (MC3E). Bull. Amer. Meteorol. Soc. http://dx.doi.org/10.1175/BAMS-D-14-00228.1.

Johnson, R.W., Kliche, D.V., Smith, P.L., 2014. Maximum likelihood estimation of gamma parameters for coarsely binned and truncated raindrop size data. Quart. J. R. Meteorol. Soc. 140 (681), 1245–1256.

Kathiravelu, G., Lucke, T., Nichols, P., 2016. Rain drop measurement techniques: a review. Water 8 (29). http://dx.doi.org/10.3390/w8010029.

Kliche, D.V., Smith, P.L, Johnson, R.W., 2008. L-moment estimators as applied to gamma drop size distributions. *J. Appl. Meteorol. Clim*. 47, 3117–3130. http://dx.doi.org/10.1175/2008JAMC1936.1.

Kottegoda, N.T., Rosso, R., 1997. Statistics, Probability, and Reliability for Civil and Environmental Engineers. McGraw-Hill, New York, USA.

Kozu, T., Iguchi, T., Kubota, T., Yoshida, N., Seto, S., Kwiatkowski, J., Takayabu, Y.N., 2009. Feasibility of raindrop size distribution parameter estimation with TRMM precipitation radar. J. Meteor. Soc. Japan 87A, 53–66. http://dx.doi.org/10.2151/jmsj.87A.53.

Kruger, A., Krajewski, W.F., 2002. Two-dimensional video disdrometer: a description. J. Atmos. Oceanic Technol. 19, 602–617. http://dx.doi.org/10.1175/1520-0426(2002)019⟨0602:TDVDAD⟩2.0.CO;2.

Laws, J.O., 1941. Measurements of the fall-velocity of water-drops and raindrops. EOS, Trans. Am. Geophys. Union 22, 709–721. http://dx.doi.org/10.1029/TR022i003p00709.

Laio, F., 2004. Cramer–von Mises and Anderson-Darling goodness of fit tests for extreme value distributions with unknown parameters. Water Res. Res. 40 (9). http://dx.doi.org/10.1029/2004WR003204.

Laio, F., Di Baldassarre, G., Montanari, A., 2009. Model selection techniques for the frequency analysis of hydrological extremes. Water Res. Res. 45 (7). http://dx.doi.org/10.1029/2007WR006666.

Lombardo, F., Volpi, E., Koutsoyiannis, D., Papalexiou, S.M., 2014. Just two moments! A cautionary note against use of high-order moments in multifractal models in hydrology. Hydrol. Earth Sist. Sci. 18, 243–255. http://dx.doi.org/10.5194/hess-18-243-2014.

Mallet, C., Barthes, L., 2009. Estimation of gamma raindrop size distribution parameters: statistical fluctuations and estimation errors. J. Atmos. Ocean. Technol. 26 (8), 1572–1584.

Marshall, J.S., Palmer, W.M., 1948. The distribution of raindrops with size. J. Meteorol. 9, 327–332. http://dx.doi.org/10.1175/1520-0469(1948)005⟨0165:TDORWS⟩2.0.CO;2.

Marzuki, M., Randeu, W.L., Kozu, T., Shimomai, T., Schönhuber, M., Hashiguchi, H., 2012. Estimation of raindrop size distribution parameters by maximum likelihood and L-moment methods: effect of discretization. Atmos. Res. 112, 1–11. http://dx.doi.org/10.1016/j.atmosres.2012.04.003.

Marzuki, M., Randeu, W.L., Kozu, T., Shimomai, T., Hashiguchi, H., Schönhuber, M., 2013. Raindrop axis ratios, fall velocities and size distribution over Sumatra from 2D-video disdrometer measurement. Atmos. Res. 119, 23–37. http://dx.doi.org/10.1016/j.atmosres.2011.08.006.

Marzuki, M., Hashiguchi, H., Kozu, T., Shimomai, T., Shibagaki, Y., Takahashi, Y., 2016. Precipitation microstructure in different Madden–Julian oscillation phases over Sumatra. Atmos. Res. 168, 121–138. http://dx.doi.org/10.1016/j.atmosres.2015.08.022.

Perrin, C., Michel, C., Andréassian, V., 2001. Does a large number of parameters enhance model performance? Comparative assessment of common catchment model structures on 429 catchments. J. Hydrol. 242, 275–301. http://dx.doi.org/10.1016/S0022-1694(00)00393-0.

Pruppacher, H.R., Klett, J.D., 1997. Microphysics of Clouds and Precipitation. Kluwer Academic Publishers, Dordrecht, The Netherlands, p. 954.

Rose, C.R., Chandrasekar, V., 2006. A GPM dual-frequency retrieval algorithm: DSD profile-optimization method. J. Atmos. Oceanic Technol. 23, 1372–1383 doi: http://dx.doi.org/10.1175/JTECH1921.1.

Rosenfeld, D., Ulbrich, C.W., 2003. Cloud microphysical properties, processes, and rainfall estimation opportunities. Meteor. Monogr. 30, 237–258. http://dx.doi.org/10.1175/0065-9401(2003)030⟨0237:CMPPAR⟩2.0.CO;2.

Salvadori, G., Tomasicchio, G.R., D'Alessandro, F., 2014. Practical guidelines for multivariate analysis and design in coastal and off-shore engineering. Coast. Eng. 88, 1–14. http://dx.doi.org/10.1016/j.coastaleng.2014.01.011.

Chapter 1 Schönhuber, M., Lammer, G., Randeu, W.L., 2008. The 2D video disdrometer. In: Michaelides, S. (Ed.), Precipitation: Advances in Measurement, Estimation and Prediction. Springer, pp. 3–31.

Schoups, G., van de Giesen, N.C., Savenije, H.H.G., 2008. Model complexity control for hydrologic prediction. Water Resour. Res. 44, W00B03. http://dx.doi.org/10.1029/2008WR006836.

Sebastianelli, S., Russo, F., Napolitano, F., Baldini, L., 2013. On precipitation measurements collected by a weather radar and a rain gauge network. Nat. Hazards Earth Syst. Sci. 13, 605–623. http://dx.doi.org/10.5194/nhess-13-605-2013.

Smith, P.L., Kliche, V.D., 2005. The bias in moment estimators for parameters of drop size distribution functions: sampling from exponential distributions. J. Appl. Meteor. 44, 1195–1205. http://dx.doi.org/10.1175/JAM2258.1.

Smith, P.L., Kliche, D.V., Johnson, R.W., 2009. The bias and error in moment estimators for parameters of drop size distribution functions: sampling from gamma distributions. J. Appl. Meteorol. Clim. 48, 2118–2126. http://dx.doi.org/10.1175/2009JAMC2114.1.

Stephens, G.L., Kummerow, C.D., 2007. The remote sensing of clouds and precipitation from space: a review. J. Atmos. Sci. 64, 3742–3765. http://dx.doi.org/10.1175/2006JAS2375.1.

Suh, S.-H., You, C.-H., Lee, D.-I., 2016. Climatological characteristics of raindrop size distributions in Busan, Republic of Korea. Hydrol. Earth Syst. Sci. 20, 193–207. http://dx.doi.org/10.5194/hess-20-193-2016.

Szyrmer, W., Laroche, S., Zawadzki, I., 2005. A microphysical bulk formulation based on scaling normalization of the particle size distribution. Part I: description. J. Atmos. Sci. 62, 4206–4221. http://dx.doi.org/10.1175/JAS3620.1.

Teugels, J., 1975. Class of subexponential distributions. Ann. Probab. 3, 1000–1011.

Testud, J., Oury, S., Black, R.A., Amayenc, P., Dou, X., 2001. The concept of "Normalized" distribution to describe raindrop spectra: a tool for cloud physics and cloud remote sensing. J. Appl. Meteor. 40, 1118–1140. http://dx.doi.org/10.1175/1520-0450(2001)040⟨1118:TCONDT⟩2.0.CO;2.

Thurai, M., Bringi, V.N., 2005. Drop axis ratios from a 2D video disdrometer. J. Atmos. Ocean. Tech. 22, 966–978. http://dx.doi.org/10.1175/JTECH1767.1.

Thurai, M., Bringi, V.N., Kennedy, P.C., Notaroš, B., Gatlin, P.N., 2015. Towards completing the rain drop size distribution spectrum: a case study involving 2d video disdrometer, droplet spectrometer, and polarimetric radar measurements in Greeley, Colorado. In: Proceedings of the 37th AMS Conference on Radar Meteorology. Norman, Oklahoma, USA.

Tokay, A., Short, D.A., 1996. Evidence from tropical raindrop spectra of the origin of rain from stratiform and convective clouds. J. Appl. Meteor. 35, 355–371. http://dx.doi.org/10.1175/1520-0450(1996)035⟨0355:EFTRSO⟩2.0.CO;2.

Tokay, A., Kruger, A., Krajewski, W.F., F., W., 2001. Comparison of drop-size distribution measurements by impact and optical disdrometers. J. Appl. Meteorol. 40, 2083–2097. http://dx.doi.org/10.1175/1520-0450(2001)040⟨2083:CODSDM⟩2.0.CO;2.

Tokay, A., Petersen, W.A., Gatlin, P., Wingo, M., 2013. Comparison of raindrop size distribution measurements by collocated disdrometers. J. Atmos. Ocean. Tech. 30, 1672–1690. http://dx.doi.org/10.1175/JTECH-D-12-00163.1.

Trenberth, K.E., 2011. Changes in precipitation with climate change. Clim. Res. 47, 123–138. http://dx.doi.org/10.3354/cr00953.

Trezzini, F., Giannella, G., Guida, T., 2013. Landslide and flood: economic and social impacts in Italy. In: Landslide science and practice. Springer, Berlin Heidelberg, pp. 171–176. http://dx.doi.org/10.1007/978-3-642-31325-7.

Ulbrich, C., 1983. Natural variations in the analytical form of the raindrop-size distribution. J. Clim. Appl. Meteorol. 22, 1764–1775. http://dx.doi.org/10.1175/1520-0450(1983)022⟨1764:NVITAF⟩2.0.CO;2.

Ulbrich, C., Atlas, D., 1998. Rainfall microphysics and radar properties: analysis methods for drop size spectra. J. Appl. Meteorol. 37, 912–923. http://dx.doi.org/10.1175/1520-0450(1998)037⟨0912:RMARPA⟩2.0.CO;2.

Vandenberghe, S., Verhoest, N.E.C., De Baets, B., 2010. Fitting bivariate copulas to the dependence structure between storm characteristics: a detailed analysis based on 105 year 10 min rainfall. Water Resour. Res. 46, W01512. http://dx.doi.org/10.1029/2009WR007857.

Van Den Heever, S.C., Cotton, W.R., 2004. The impact of hail size on simulated supercell storms. *J. Atmos. Sci.* 61, 1596–1609. http://dx.doi.org/10.1175/1520-0469(2004)061⟨1596:TIOHSO⟩2.0.CO;2.

Villarini, G., Krajewski, W.F., 2010. Review of the different sources of uncertainty in single polarization radar-based estimates of rainfall. Surv. Geophys. 31, 107–129. http://dx.doi.org/10.1007/s10712-009-9079-x.

Waldvogel, A., 1974. The N_0 jump of raindrop spectra. J. Atmos. Sci. 31, 1067–1078. http://dx.doi.org/10.1175/1520-0469(1974)031⟨1067:TJORS⟩2.0.CO;2.

Williams, C.R., et al., 2014. Describing the shape of raindrop size distributions using uncorrelated raindrop mass spectrum parameters. J. Appl. Meteor. Climatol. 53, 1282–1296. http://dx.doi.org/10.1175/JAMC-D-13-076.1.

Zucchini, W., 2000. An introduction to model selection. J. Math. Psychol. 44, 41–61. http://dx.doi.org/10.1006/jmps.1999.1276.